

Phenomenology of the minimal $B - L$ extension of the Standard model: Z' and neutrinos

Lorenzo Basso^{1,2}, Alexander Belyaev^{1,2}, Stefano
Moretti^{1,2} and Claire H. Shepherd-Themistocleous²

¹ *School of Physics & Astronomy, University of Southampton,
Highfield, Southampton SO17 1BJ, UK*

² *Particle Physics Department, Rutherford Appleton Laboratory,
Chilton, Didcot, Oxon OX11 0QX, UK*

We present the Large Hadron Collider (LHC) discovery potential in the Z' and heavy neutrino sectors of a $U(1)_{B-L}$ enlarged Standard Model also encompassing three heavy Majorana neutrinos. This model exhibits novel signatures at the LHC, the most interesting arising from a Z' decay chain involving heavy neutrinos, eventually decaying into leptons and jets. In particular, this signature allows one to measure the Z' and heavy neutrino masses involved. In addition, over a large region of parameter space, the heavy neutrinos are rather long-lived particles producing distinctive displaced vertices that can be seen in the detectors. Lastly, the simultaneous measurement of both the heavy neutrino mass and decay length enables an estimate of the absolute mass of the parent light neutrino.

I. INTRODUCTION

The $B - L$ (baryon number minus lepton number) symmetry plays an important role in various physics scenarios beyond the Standard Model (SM). Firstly, the gauged $U(1)_{B-L}$ symmetry group is contained in a Grand Unified Theory (GUT) described by a $SO(10)$ group [1]. Secondly, the scale of the $B - L$ symmetry breaking is related to the mass scale of the heavy right-handed Majorana neutrino mass terms providing the well-known see-saw mechanism [2] of light neutrino mass generation. Thirdly, the $B - L$ symmetry and the scale of its breaking are tightly connected to the baryogenesis mechanism through leptogenesis [3] via sphaleron interactions preserving $B - L$.

In the present paper we study the minimal $B-L$ low-energy extension of the SM consisting of a further $U(1)_{B-L}$ gauge group, three right-handed neutrinos and an additional Higgs boson generated through the $U(1)_{B-L}$ symmetry breaking. It is important to note that in this model the $B - L$ breaking can take place at the Electro-Weak (EW) or TeV scale, i.e., a value far below that of any GUT scale. This $B - L$ scenario therefore has potentially interesting signatures at hadron colliders, particularly the LHC. New particle states such as Z' , Higgses and neutrinos, all naturally have masses at the EW or TeV scale. The breaking of the $B - L$ symmetry at the EW or TeV scale can be viewed as a remnant of a grand unified gauge symmetry, such as $SO(10)$. Furthermore, with respect to baryogenesis, since $B + L$ is violated by sphaleron interactions, this implies that baryogenesis or leptogenesis cannot occur above the scale of $B - L$ breaking. A scenario with $B - L$ breaking at the EW (or TeV) scale therefore implies EW (or TeV) scale baryogenesis [4].

The particular subject of the present paper is the first detailed study of the collider phenomenology of the gauge and fermionic sectors of the minimal $B - L$ extension of the SM, where the additional $U(1)_{B-L}$ gauge group is indeed associated to the $B - L$ number [1, 5, 6]. The analysis of the scalar sector will appear in a future paper [7]. The new results on $B - L$ phenomenology at the LHC include observable signals from a Z' -boson as well as heavy neutrinos with a mass of up to several hundred GeV¹. A very interesting feature of such a $B - L$ model is possibly relatively long lifetimes of the heavy neutrinos which can directly be measured. In turn, such a measurement could be a key to shedding light on the

¹ We deliberately assume that the $B - L$ symmetry breaking scale generating $M_{Z'}$ is somewhat higher than the scale of the heavier right-handed neutrino mass, thereby enabling Z' to heavy neutrino decays.

mass spectra of the light neutrinos.

This work is organised as follows. Sect. II reviews the model under study and its implementation in the CalcHEP package [8], together with an overview of its parameter space. Sects. III A and III B study the decay properties – specifically, width and Branching Ratios (BRs) – of the new spin-1 and spin-1/2 particles of the $B - L$ model. Sect. III C discusses their experimental signatures and production plus decay cross sections and also contains a numerical analysis for two particular benchmark points in the $B - L$ parameter space, followed by a study of the expected background. The conclusions are in Sec. IV.

II. THE $B - L$ MODEL AND ITS IMPLEMENTATION INTO CALCHEP

A. The model

The model under study is the so-called “pure” or “minimal” $B - L$ model (see [6] for conventions and references) since it has vanishing mixing between the two $U(1)_Y$ and $U(1)_{B-L}$ groups. In the rest of this paper we refer to this model simply as the “ $B - L$ model”. In this model the classical gauge invariant Lagrangian, obeying the $SU(3)_C \times SU(2)_L \times U(1)_Y \times U(1)_{B-L}$ gauge symmetry, can be decomposed as:

$$\mathcal{L} = \mathcal{L}_{YM} + \mathcal{L}_s + \mathcal{L}_f + \mathcal{L}_Y. \quad (1)$$

The non-Abelian field strengths in \mathcal{L}_{YM} are the same as in the SM whereas the Abelian ones can be written as follows:

$$\mathcal{L}_{YM}^{\text{Abel}} = -\frac{1}{4}F^{\mu\nu}F_{\mu\nu} - \frac{1}{4}F'^{\mu\nu}F'_{\mu\nu}, \quad (2)$$

where

$$F_{\mu\nu} = \partial_\mu B_\nu - \partial_\nu B_\mu, \quad (3)$$

$$F'_{\mu\nu} = \partial_\mu B'_\nu - \partial_\nu B'_\mu. \quad (4)$$

In this field basis, the covariant derivative is:

$$D_\mu \equiv \partial_\mu + ig_S T^\alpha G_\mu^\alpha + ig T^a W_\mu^a + ig_1 Y B_\mu + ig'_1 Y_{B-L} B'_\mu. \quad (5)$$

The fermionic Lagrangian (where k is the generation index) is given by

$$\begin{aligned} \mathcal{L}_f = \sum_{k=1}^3 & \left(i\overline{q_{kL}}\gamma_\mu D^\mu q_{kL} + i\overline{u_{kR}}\gamma_\mu D^\mu u_{kR} + i\overline{d_{kR}}\gamma_\mu D^\mu d_{kR} + \right. \\ & \left. + i\overline{l_{kL}}\gamma_\mu D^\mu l_{kL} + i\overline{e_{kR}}\gamma_\mu D^\mu e_{kR} + i\overline{\nu_{kR}}\gamma_\mu D^\mu \nu_{kR} \right), \end{aligned} \quad (6)$$

with the respective fermion charges given in Tab. I. The $B - L$ charge assignments of new fields as well as the introduction of new scalar Higgs (χ) and fermionic right-handed heavy neutrinos (ν_R) fields are designed to eliminate the triangle $B - L$ gauge anomalies. (Tab. II shows the scalar content and charges of our $B - L$ model.) Therefore, the $B - L$ gauge extension of the SM group broken at the EW scale does necessarily require at least one new scalar field and three new fermionic fields which are charged with respect to the $B - L$ group.

The scalar Lagrangian is:

$$\mathcal{L}_s = (D^\mu H)^\dagger D_\mu H + (D^\mu \chi)^\dagger D_\mu \chi - V(H, \chi), \quad (7)$$

with the scalar potential given by

$$V(H, \chi) = m^2 H^\dagger H + \mu^2 |\chi|^2 + \lambda_1 (H^\dagger H)^2 + \lambda_2 |\chi|^4 + \lambda_3 H^\dagger H |\chi|^2, \quad (8)$$

where H and χ are the complex scalar Higgs doublet and singlet fields, respectively.

Finally, the Yukawa interactions are:

$$\begin{aligned} \mathcal{L}_Y = & -y_{jk}^d \overline{q_{jL}} d_{kR} H - y_{jk}^u \overline{q_{jL}} u_{kR} \tilde{H} - y_{jk}^e \overline{l_{jL}} e_{kR} H \\ & - y_{jk}^\nu \overline{l_{jL}} \nu_{kR} \tilde{H} - y_{jk}^M \overline{(\nu_R)_j}^c \nu_{kR} \chi + \text{h.c.}, \end{aligned} \quad (9)$$

where $\tilde{H} = i\sigma^2 H^*$ and i, j, k take the values 1 to 3, where the last term is the Majorana contribution and the others the usual Dirac ones.

B. Model implementation into CalcHEP

We make use of the CalcHEP package [8] to study the collider phenomenology of the $B - L$ model. For the derivation of the Feynman rules (see the Appendix for those pertaining to the heavy neutrino interactions) and for the straightforward implementation of the model in the CalcHEP package, we have used the LanHEP module [9]. The availability of the model

ψ	$SU(3)_C$	$SU(2)_L$	Y	$B - L$
q_L	3	2	$\frac{1}{6}$	$\frac{1}{3}$
u_R	3	1	$\frac{2}{3}$	$\frac{1}{3}$
d_R	3	1	$-\frac{1}{3}$	$\frac{1}{3}$
l_L	1	2	$-\frac{1}{2}$	-1
e_R	1	1	-1	-1
ν_R	1	1	0	-1

TABLE I: Fermion content and charges for the $B - L$ model.

ψ	$SU(3)_C$	$SU(2)_L$	Y	$B - L$
H	1	2	$\frac{1}{2}$	0
χ	1	1	0	2

TABLE II: Scalar content and charges for the $B - L$ model.

implementation into CalcHEP in both the unitary and t'Hooft-Feynman gauges allowed us to perform powerful cross-checks to test the consistency of the model itself.

The implementation of the gauge sector is quite straightforward. Since there is no mixing between the (SM) Z and Z_{B-L} bosons (hereafter, we will refer to the Z_{B-L} boson as a Z') one just needs to define a new heavy neutral gauge boson together with the covariant derivative given by eq. (5) and the charge assignments in Tabs. I–II. For the scalar sector, we need to implement the mixing between mass and gauge eigenstates of the two Higgs bosons.

The implementation of the neutrino sector is somewhat more complicated. Majorana-

like Yukawa terms are present in eq. (9) for the right-handed neutrinos, therefore one must implement this sector such that the gauge invariance of the model is explicitly preserved. This can be done as follows. As a first step we rewrite Dirac neutrino fields in terms of Majorana ones using the following general substitution:

$$\nu^D = \frac{1 - \gamma_5}{2} \nu_L + \frac{1 + \gamma_5}{2} \nu_R, \quad (10)$$

where ν^D is a Dirac field and $\nu_{L(R)}$ are its left (right) Majorana components. If we perform the substitution of eq. (10) in the neutrino sector of the SM, we will have an equivalent theory formulated in terms of Majorana neutrinos consistent with all experimental constraints.

The second step is to diagonalise the neutrino mass matrix from eq. (9):

$$\mathcal{M} = \begin{pmatrix} 0 & m_D \\ m_D & M \end{pmatrix}, \quad (11)$$

where

$$m_D = \frac{y^\nu}{\sqrt{2}} v, \quad M = \sqrt{2} y^M x, \quad (12)$$

where x is the Vacuum Expectation Value (VEV) of the χ field. This matrix can be diagonalised by a rotation about an angle α_ν , such that:

$$\tan 2\alpha_\nu = -\frac{2m_D}{M}. \quad (13)$$

For simplicity we neglect the inter-generational mixing so that neutrinos of each generation can be diagonalised independently. We also require that the neutrinos be mass degenerate. Thus, $\nu_{L,R}$ can be written as the following linear combination of Majorana mass eigenstates $\nu_{l,h}$:

$$\begin{pmatrix} \nu_L \\ \nu_R \end{pmatrix} = \begin{pmatrix} \cos \alpha_\nu & -\sin \alpha_\nu \\ \sin \alpha_\nu & \cos \alpha_\nu \end{pmatrix} \times \begin{pmatrix} \nu_l \\ \nu_h \end{pmatrix}. \quad (14)$$

The last subtle point is the way the Lagrangian has to be written, in particular the Majorana-like Yukawa terms for the right-handed neutrinos (the last term in eq. (9)). In order to explicitly preserve gauge invariance, this term has to be written, in two-component notation, as:

$$-y^M \nu^c \frac{1 + \gamma_5}{2} \nu \chi + \text{h.c.}, \quad (15)$$

where ν is the Dirac field of eq. (10), whose Majorana components $\nu_{L,R}$ mix as in eq. (14).

C. Parameter space

In this section we define the independent parameters of the $B - L$ model and their valid range². The set of parameters relevant to our study is the following one.

- g'_1 , the new $U(1)_{B-L}$ gauge coupling. Here, the absence of a Landau pole up to the GUT scale $Q_{GUT} = 10^{16}$ GeV implies $g'_1 < 0.5$ from a Renormalisation Group Equation (RGE) analysis [6, 10].
- $M_{Z'}$, the new gauge boson mass. An indirect constraint on $M_{Z'}$ comes from analyses at the Large Electron-Positron (LEP) collider of Fermi effective four-fermions interactions [11]:

$$\frac{M_{Z'}}{g'_1} \geq 6 \text{ TeV}. \quad (16)$$

As we demonstrate below, this constraint will provide an upper bound to the Z' production cross sections at the LHC.

- M_{ν_h} , the heavy neutrino masses. We take them to be degenerate and relatively light, varying in the range $50 \text{ GeV} < M_{\nu_h} < 500 \text{ GeV}$.
- m_{ν_l} , the SM (or light) neutrino masses. We use the cosmological upper bound $\sum_l m_{\nu_l} < 1 \text{ eV}$. As we will see in Sect. III A, detectable displaced vertices may occur for $m_{\nu_l} \lesssim 10^{-2} \text{ eV}$.

For this analysis of the collider phenomenology of our $B - L$ model we have chosen $M'_Z = 1.5 \text{ TeV}$ and $g'_1 = 0.2$ as a representative point satisfying present experimental constraints as well as two values for heavy neutrino masses: $M_{\nu_h} = 200$ and 500 GeV . Finally, we have fixed the light neutrino mass to be $m_{\nu_l} = 10^{-2} \text{ eV}$. For illustrative purposes we take all neutrino masses, both light and heavy, to be degenerate.

² Since the scalar sector is not within the scope of the present study we do not discuss the corresponding parameters, as one can choose settings in parameter space such that the scalars are entirely decoupled from the remaining particles. Here, we achieve this by requiring $\lambda_1 = 3$, $\lambda_2 = 0.08$ and $\lambda_3 = 0.01$, so that the scalars masses are $m_{h_1} \approx 600 \text{ GeV}$ and $m_{h_2} \approx 1.5 \text{ TeV}$, corresponding to our default benchmark parameters in the Z' sector, $g'_1 = 0.2$, $M_{Z'} = 1.5 \text{ TeV}$. The only exceptions to this will be made in Sects. III A and III B, where we will temporarily adopt other settings, to describe the complete decay pattern of the Z' and heavy neutrinos.

III. PHENOMENOLOGY OF THE $B - L$ MODEL

A. Heavy neutrino properties

1. Heavy neutrino decays

After the diagonalisation of the neutrino mass matrix realising the see-saw mechanism, we obtain three very light neutrinos (ν_l), which are the SM-like neutrinos, and three heavy neutrinos (ν_h). The latter have an extremely small mixing with the ν_l 's thereby providing very small but non-vanishing couplings to gauge and Higgs bosons (see the Appendix for the Feynman rules involving heavy neutrino interactions) which in turn enable the following ν_h decays: $\nu_h \rightarrow l^\pm W^\mp$, $\nu_h \rightarrow \nu_l Z$, $\nu_h \rightarrow \nu_l h_1$, $\nu_h \rightarrow \nu_l h_2$ as well as $\nu_h \rightarrow \nu_l Z'$ when these decay channels are kinematically allowed. Fig. 1 presents the corresponding BRs versus

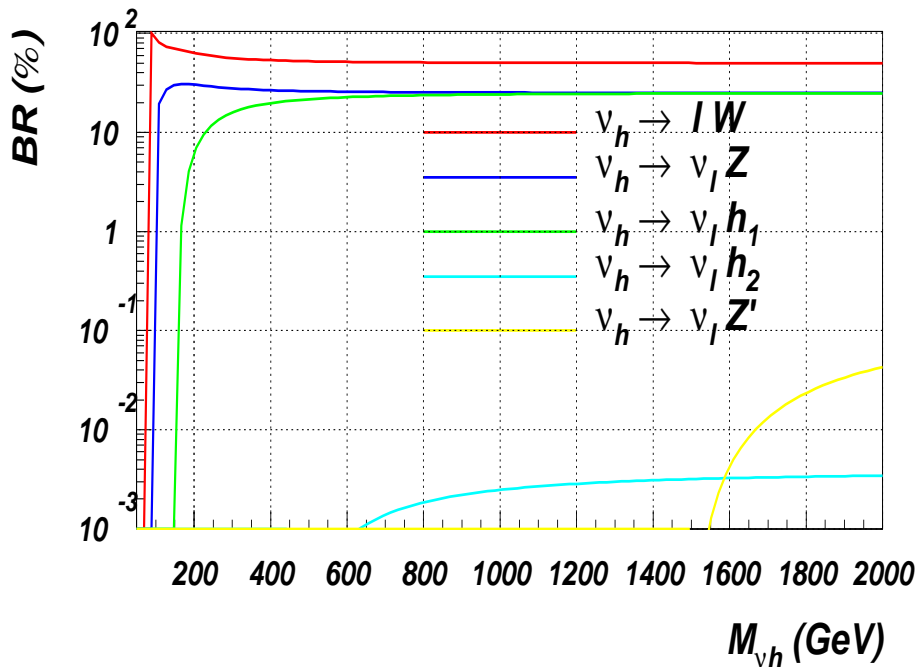


FIG. 1: Heavy neutrino branching ratios versus its mass for the fixed $M_{Z'} = 1.5$ TeV, $m_{h_1} = 150$ GeV and $m_{h_2} = 450$ GeV corresponding to $\lambda_1 = 0.19$, $\lambda_2 = 0.017$, $\lambda_3 = 0.01$ and $g'_1 = 0.2$. Here, W means the sum over W^+ and W^- .

the heavy neutrino mass for the values of the other relevant B_L parameters given in the

caption. One can see that the $BR(\nu_h \rightarrow l^\mp W^\pm)$ is dominant and reaches the 2/3 level in the $M_{\nu_h} \gg M_W, M_Z$ limit, while $BR(\nu_h \rightarrow \nu_l Z)$ and $BR(\nu_h \rightarrow \nu_l h_1)$ both reach the 1/6 level in this regime. In contrast, the $\nu_h \rightarrow \nu_l h_2$ as well as $\nu_h \rightarrow \nu_l Z'$ decay channels are well below the percent level and are negligible for our study. In this paper we will eventually assume that the heavy neutrino masses are smaller than both Higgs boson masses. Under this assumption $\nu_h \rightarrow \nu_l h_i$ ($i = 1, 2$) is not kinematically possible and $BR(\nu_h \rightarrow \nu_l Z)$ reaches the 1/3 level in the $m_{\nu_h} \gg M_W, M_Z$ limit.

2. Lifetime of the heavy neutrinos

The heavy neutrino couplings to the weak gauge bosons are proportional to the ratio of light and heavy neutrino masses (see the Appendix), which is extremely small. Therefore the decay width of the heavy neutrino is correspondingly small and its lifetime large. The heavy neutrino can therefore be a long lived particle and, over a large portion of parameter space, its lifetime can be comparable to or exceed that of the b -quark. (In fact, for $m_{\nu_l} = 10^{-2}$ eV and $M_{\nu_h} = 200$ GeV they are equal.) In Fig. 2 we present the heavy neutrino lifetime (top) in pico-seconds and the proper decay length (or mean path) (bottom) in micro-meters as a function of the light neutrino mass. The proper decay length is defined as $c\tau_0$, where τ_0 is the lifetime of the heavy neutrino. The purple band presents the proper decay length of the b -quark while the blue band indicates the range of a typical micro-vertex detector. The red band shows the region of light neutrino masses excluded by direct measurements of neutrino oscillations [12], by taking the lighter neutrino to be massless (so that the other neutrinos cannot populate this region). One should also note that the lifetime and the proper decay length of the heavy neutrinos in the laboratory frame will actually be equal to those given in Fig. 2 times the Lorentz factor equal to p_{ν_h}/M_{ν_h} defined by the ratio $M_{Z'}/M_{\nu_h}$ which can be as large as about a factor of 10. We can then see that there exists a region where the heavy neutrino lifetime is of the same order as that of the b -quark (shown as a purple band). The mean path and the respective lifetime of heavy neutrinos can therefore be measured from a displaced vertex inside the detector. The heavy neutrino can however be distinguished from a b -hadron through the observation of vertices consisting of only two isolated leptons. (A SM B -meson decay while possible would have a very small BR, $\sim 10^{-8}$ at the most.)

An experimentally resolvable non-zero lifetime along with a mass determination for the

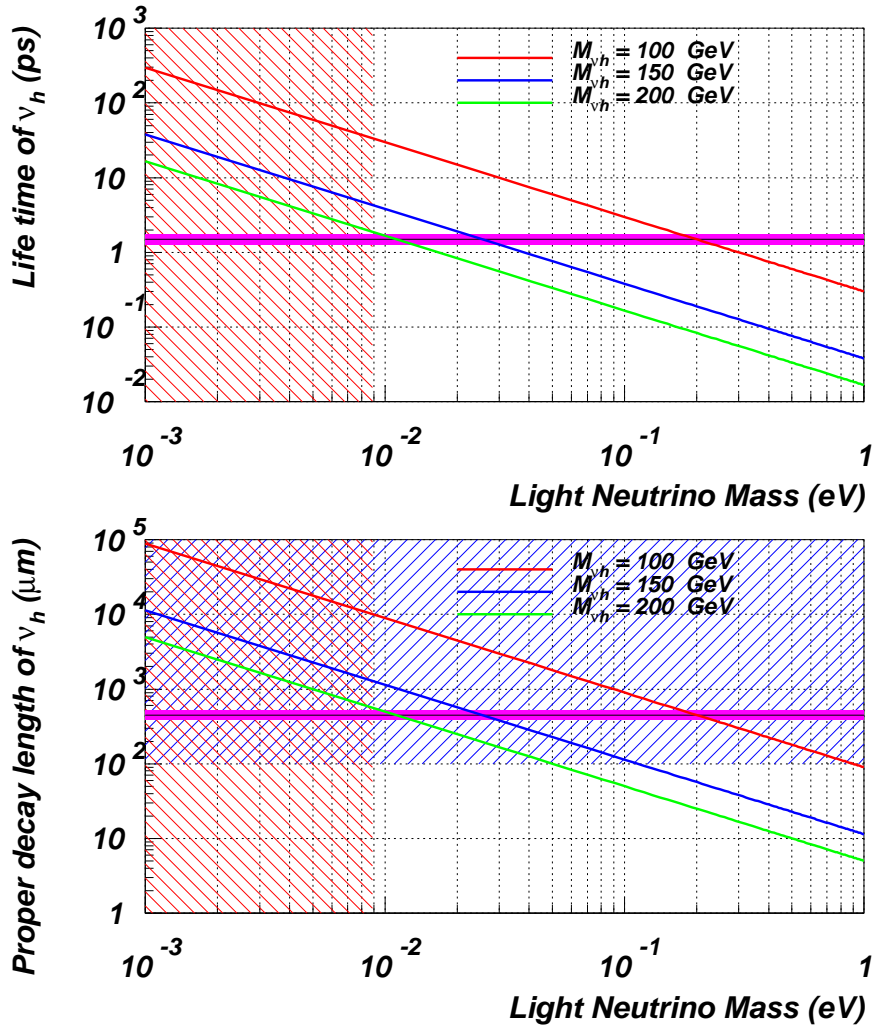


FIG. 2: Heavy neutrino life-time (top) and proper decay length (or mean path) $c\tau_0$ (bottom) as a function of the light neutrino mass. The purple band presents the proper decay length of the b -quark while the blue band indicates the range of a typical micro-vertex detector. The red band shows the region excluded by neutrino oscillation direct measurements.

heavy neutrino also enables a determination of the light neutrino mass. The lifetime measurement allows the small heavy-light neutrino mixing to be determined and as one can see from eqs. (11)–(14) this, along with the heavy neutrino mass, gives the light neutrino mass. Considering only one generation for simplicity, this is expanded upon below.

Mass eigenstates are related to gauge eigenstates by eq. (14), hence the eigenvalues are

given by solving the equation:

$$\begin{pmatrix} m_{\nu_l} & 0 \\ 0 & M_{\nu_h} \end{pmatrix} = \begin{pmatrix} c_\nu & s_\nu \\ -s_\nu & c_\nu \end{pmatrix} \begin{pmatrix} 0 & m_D \\ m_D^T & M \end{pmatrix} \begin{pmatrix} c_\nu & -s_\nu \\ s_\nu & c_\nu \end{pmatrix},$$

which yields

$$m_{\nu_l} = \sin 2\alpha_\nu m_D + \sin^2 \alpha_\nu M, \quad (17)$$

$$M_{\nu_h} = -\sin 2\alpha_\nu m_D + \cos^2 \alpha_\nu M, \quad (18)$$

with α_ν given by eq. (13). We have then three parameters (m_D , M and α_ν) and a constraint (given by eq. (13)), that can be used to eliminate one parameter from the above equations.

The Feynman rules given in the Appendix demonstrate that heavy neutrino interactions are determined by the mixing angle α_ν only, as is the total width (and therefore the mean decay length). Hence, it is convenient to keep M_{ν_h} and α_ν as independent model parameters eliminating m_D from eq. (13),

$$m_D = m_D(\alpha_\nu, M_{\nu_h}). \quad (19)$$

By measuring the heavy neutrino mass we can also invert eq. (18)

$$M = M(\alpha_\nu, M_{\nu_h}), \quad (20)$$

to finally get a fully known expression for the SM light neutrino mass as a function of our input parameters M_{ν_h} and α_ν , that we can measure independently, by inserting eqs. (19)–(20) into eq. (17),

$$m_{\nu_l}(m_D, M) = m_{\nu_l}(\alpha_\nu, M_{\nu_h}). \quad (21)$$

This simple picture shows that within the $B - L$ model we have an indirect way of accessing the SM light neutrino mass by measuring the mass of the heavy neutrino and the kinematic features of its displaced vertex. If the whole structure of mixing is taken into account, including inter-generational mixing in the heavy neutrino sector, the task of determining the light neutrino mass this way would become more complicated but the qualitative features and the overall strategy would remain the same thereby providing one with a unique link between very large and very small mass objects.

B. Z' decay properties

As discussed earlier, the extra $U(1)_{B-L}$ gauge group provides an additional neutral gauge boson, Z' , with no mixing with the SM Z -boson. Therefore our Z' boson decays only to fermions at tree-level and its width is given by the following expression:

$$\Gamma(Z' \rightarrow f\bar{f}) = \frac{M_{Z'}}{12\pi} C_f (v^f)^2 \left[1 + 2 \frac{m_f^2}{M_{Z'}^2} \right] \sqrt{1 - \frac{4m_f^2}{M_{Z'}^2}}, \quad (22)$$

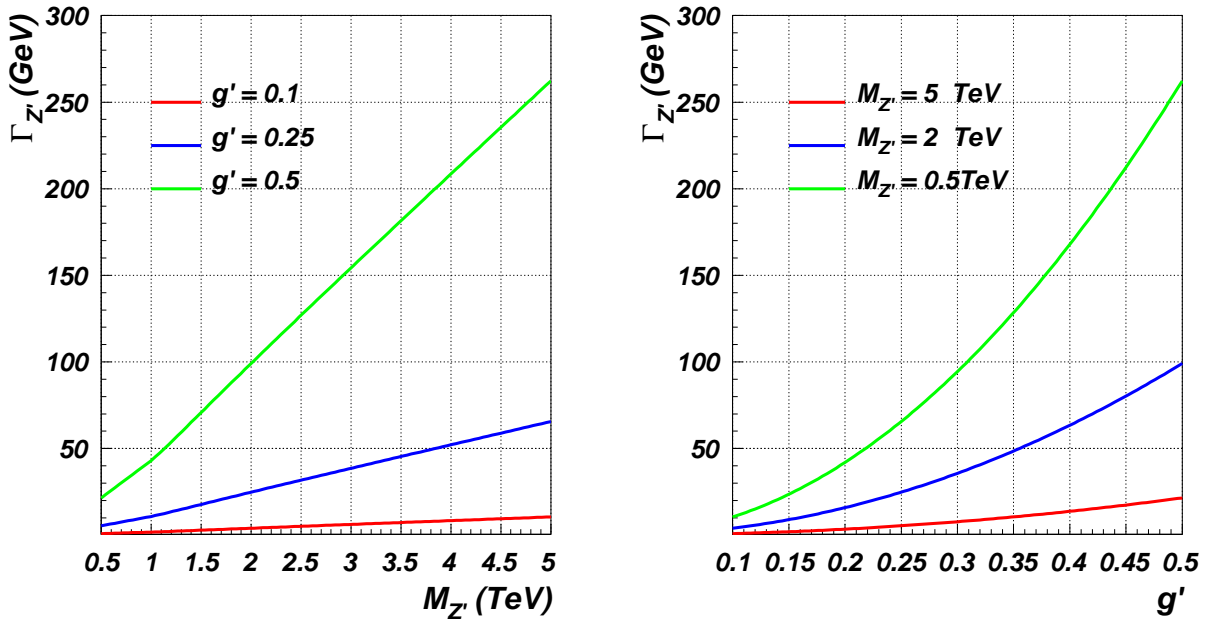
where m_f is the mass and C_f the number of colours of the fermion type f and $v^f = (B - L) \times g'_1$ is the vector coupling (see Tab. I).

In Figs. 3(a) and 3(b) we present the total decay width of the Z' as a function of $M_{Z'}$ and g'_1 , respectively (with the other parameters held fixed to three different values), assuming that the partial decay width into heavy neutrinos vanishes. Also, Fig. 3(c) presents the relative variation of the total width as a function of the ν_h mass for three different values of $M_{Z'}$ and with $g'_1 = 0.5$.

From the first two plots we see that the total width of a Z' gauge boson varies from a few to hundreds of GeV over a mass range of $0.5 \text{ TeV} < M_{Z'} < 5 \text{ TeV}$, depending on the value of g'_1 , while from the third plot one can gather the importance of taking into consideration the heavy neutrinos, since their relative contribution to the total width can be as large as 25% (whenever this channel is open). One should also note that possible Z' decays into one light and one heavy neutrino are highly suppressed by the corresponding (heavy-light) neutrino mixing and thus they can safely be neglected.

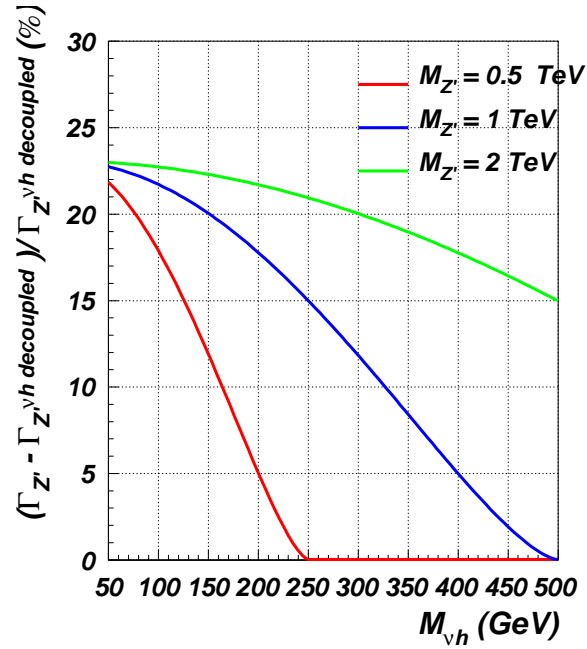
The possibility of decays of the Z' gauge boson into pairs of heavy neutrinos is one of the most significant results of this work since, in addition to the clean SM-like di-lepton signature, it provides multi-lepton signatures where backgrounds can strongly be suppressed. In order to address this quantitatively, we first determine the relevant BRs. Clearly, these depend strongly on the heavy neutrino mass and Fig. 4 shows how they change with fixed (although arbitrary) values of M_{ν_h} , for the following three cases: a heavy neutrino (i) much lighter than, (ii) lighter than and (iii) comparable in mass to the Z' , in the range $0.5 \text{ TeV} < M_{Z'} < 5 \text{ TeV}$, before summing over generations.

A feature of the current $B - L$ model illustrated in the previous figures is that the Z' predominantly couples to leptons. In fact, after summing over the generations, $k = 1 \dots 3$, we



(a)

(b)



(c)

FIG. 3: Z' total width as a function of: 3(a) $M_{Z'}$ (for fixed values of g'_1), 3(b) g'_1 (for fixed values of $M_{Z'}$) and 3(c) M_{ν_h} (for fixed values of $M_{Z'}$ and $g'_1 = 0.5$).

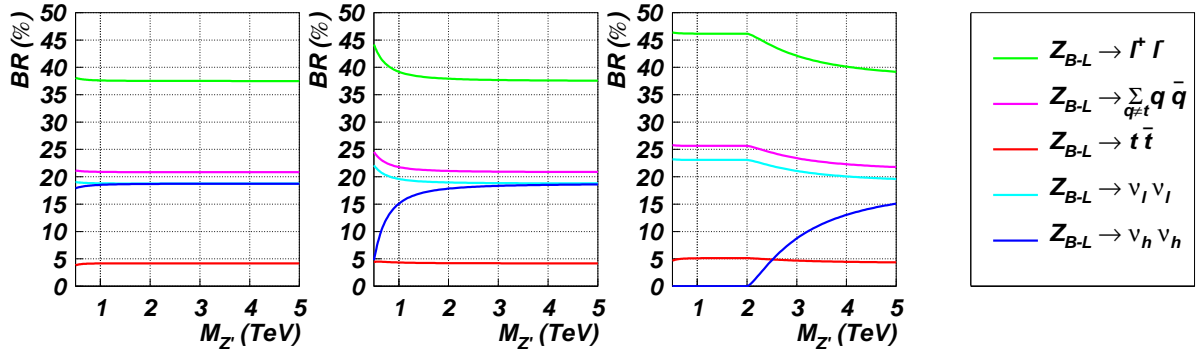


FIG. 4: Z' BRs as a function of $M_{Z'}$ for several heavy neutrino masses: $M_{\nu_h} = 50, 200$ and 1000 GeV, from left to right, respectively. A summation over all lepton/neutrino flavours is implied throughout whereas in the case of quarks we distinguish between light flavours ($q = d, u, s, c, b$) and the top quark.

roughly get for leptons and quarks:

$$\sum_k BR(Z' \rightarrow l_k \bar{l}_k + \nu_k \bar{\nu}_k) \sim \frac{3}{4}, \quad \sum_k BR(Z' \rightarrow q_k \bar{q}_k) \sim \frac{1}{4}.$$

Not surprisingly then, for a relatively light (with respect to the Z' gauge boson) heavy neutrino, the Z' BR into pairs of such particles is relatively high: $\sim 18\%$ (at most, again, after summing over the generations).

Combining this last result together with those of Sect. III B, we can discuss an interesting feature of the $B-L$ model, namely, the multi-lepton signatures (meaning two or more leptons being involved). A single heavy neutrino decay will produce a signature of 0, 1 or 2 charged leptons, depending on whether the heavy neutrino decays via a charged or neutral current and on the subsequent decays of the SM W^\pm and Z gauge bosons. We can have both chains

$$\nu_h \rightarrow l^\pm W^\mp \rightarrow l^\pm + \begin{cases} l^\mp \nu_l \\ \text{hadrons} \end{cases} \quad (23)$$

and

$$\nu_h \rightarrow \nu_l Z \rightarrow \nu_l + \begin{cases} l^+ l^- \\ \nu_l \nu_l / \text{hadrons} \end{cases}. \quad (24)$$

The pattern in (23) provides 1 or 2 charged leptons whilst that in (24) zero or 2, so that multi-lepton signatures may arise when the Z' gauge boson decays into a pair of heavy neutrinos, producing up to four charged leptons in the final state. Fig. 5 shows the BRs of a

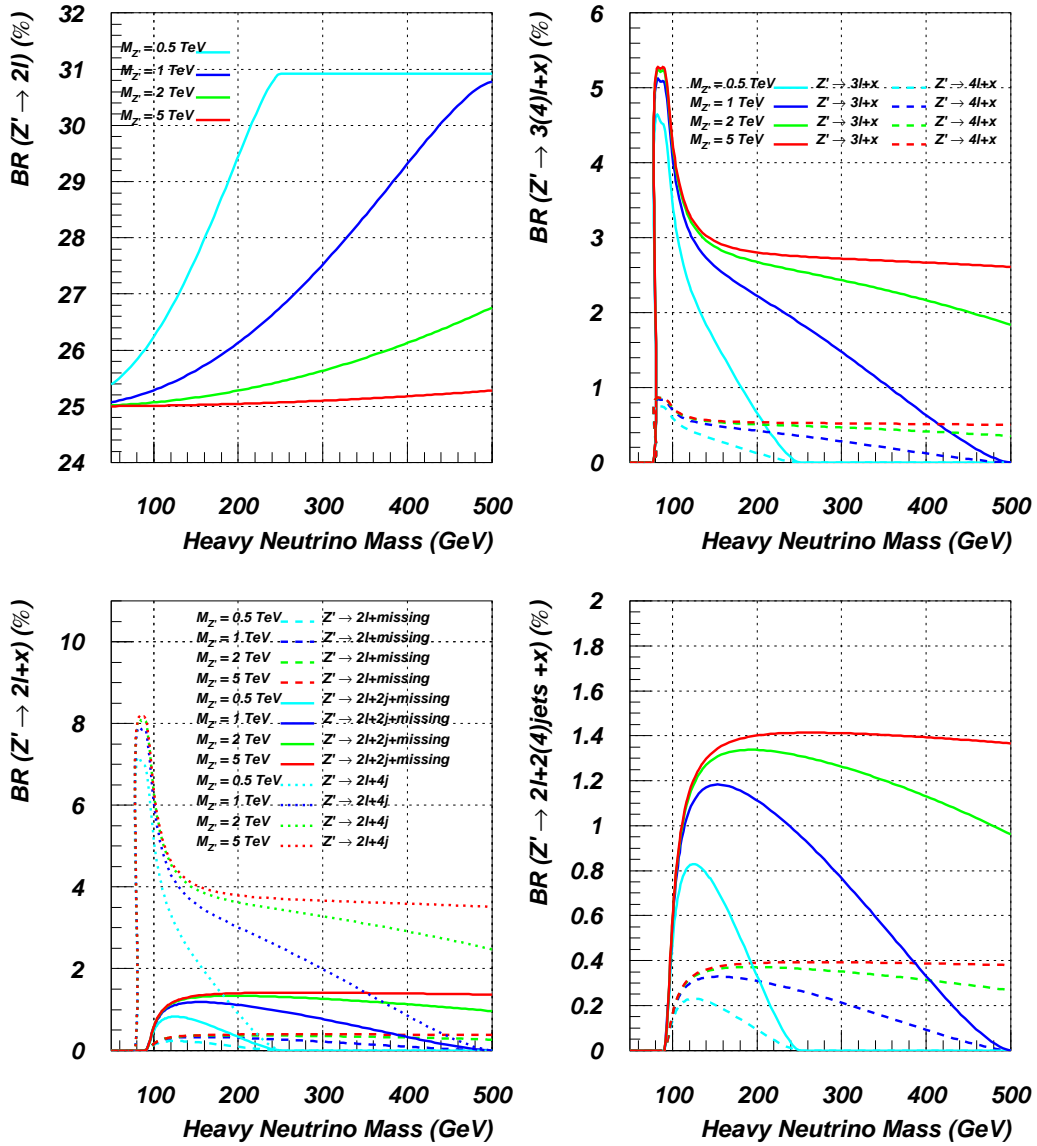


FIG. 5: Z' BRs, as a function of M_{ν_h} , into: 2 leptons (both e and μ , top-left); 3 and 4 leptons + X (both e and μ , top-right); 2 leptons + X jets (both e and μ , bottom-left); zoom of the previous plot with same legend (bottom-right).

Z' decaying into 2 (top-left) and 3 or 4 (top-right) leptons (plus possibly missing transverse momentum and/or jets, as appropriate) as a function of M_{ν_h} , where a lepton can be either an electron or a muon and these contributions are summed. While the former are clearly dominant the latter are not at all negligible. For $M_{W^\pm} < M_{\nu_h} < M_{Z'}$, the $\nu_h \rightarrow l^\mp W^\pm$

decay is the only one kinematically possible whereas for $M_{\nu_h} < M_{W^\pm}$ the heavy neutrino can decay only via an off shell W and is therefore very long lived. For a very massive Z' ($2 \text{ TeV} < M_{Z'} < 5 \text{ TeV}$) the multi-leptonic BRs are roughly 2.5% in the case of $Z' \rightarrow 3l$ and 0.5% in the case of $Z' \rightarrow 4l$, for a wide range of heavy neutrino masses.

Finally, from (23) and (24) one can see that di-lepton decays are possible, whereas Z' decays give rise to 2 leptons plus a large amount of missing transverse momentum and/or highly energetic jets: see Fig. 5 (bottom-left). Particularly interesting is the decay into 2 leptons and 4 jets, since here there is no missing transverse momentum at all and its BR is rather large with respect to the other non-SM signatures, as we can see in Fig. 5 (bottom-left).

C. Signal-to-background analysis

In this section we perform a signal-to-background analysis to check the observability at the LHC of some of the signatures discussed that may originate from the present $B - L$ model.

In our model setup, wherein the scalar sector is entirely decoupled, all interesting $B - L$ signals come from Z' production, since the Z' is the only new particle whose couplings to the SM partons are large. The most efficient hadro-production process involving a Z' boson is the Drell-Yan (DY) mode

$$q\bar{q} \rightarrow Z', \quad (25)$$

where q is either a valence-quark or a sea-quark in the proton. At the parton level, the Z' production cross section for process (25) depends on two main parameters: $M_{Z'}$ and g'_1 . In Fig. 6(a) we present the Z' hadro-production cross section σ at the LHC as a function of both $M_{Z'}$ and g'_1 , in the ranges $0.5 \text{ TeV} < M_{Z'} < 5 \text{ TeV}$ and $0.1 < g'_1 < 0.5$, respectively, while Fig. 6(b) presents the contour levels in the $(M_{Z'}, g'_1)$ plane for $\sigma = 4 \text{ pb}$, 0.3 pb , 50 fb and 5 fb . The shaded area in Fig. 6(b) is excluded by eq. (16).

We expect that the LHC will discover a Z' boson from our $B - L$ model in the standard di-lepton decay channel. In Fig. 7 we therefore show the Z' line-shape, i.e., the differential cross section for process (25) as a function of the invariant mass of its decay products, e.g., as obtained from the Z' decay into a pair of muons:

$$q\bar{q} \rightarrow Z' \rightarrow \mu^+ \mu^-, \quad (26)$$

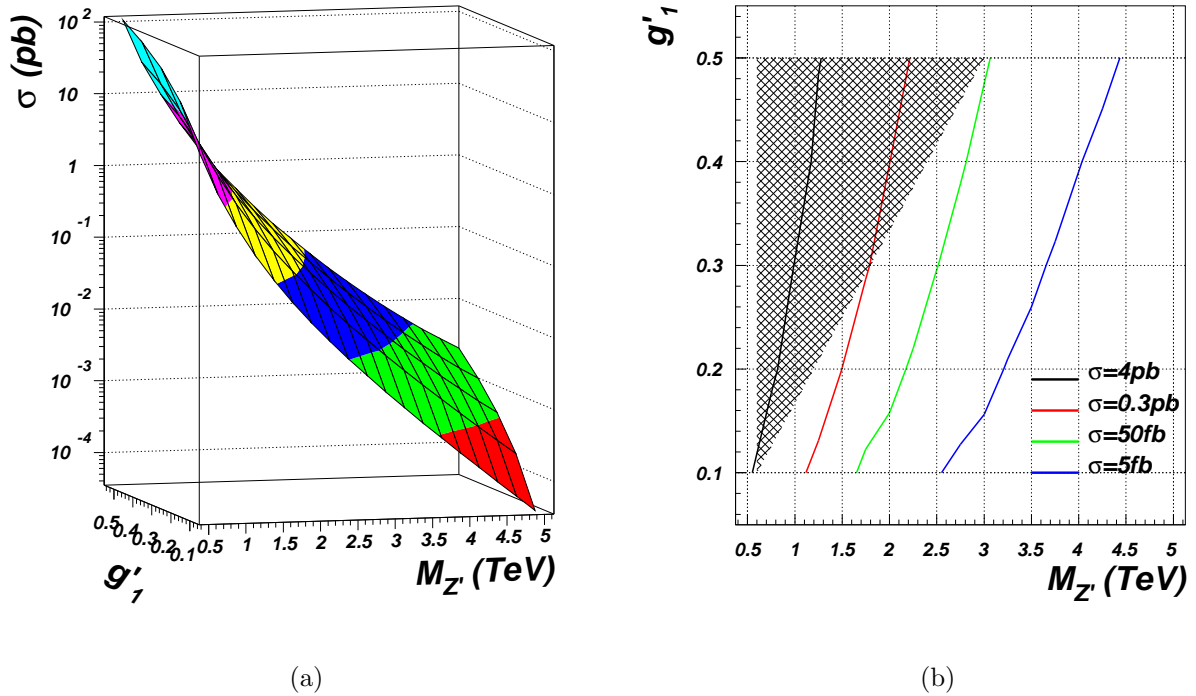


FIG. 6: Z' hadro-production cross section at the LHC over the $(M_{Z'}, g'_1)$ plane: 6(a) as a continuous function of $M_{Z'}$ and g'_1 and 6(b) in the form of contour lines for four fixed values of production rates. The dark shaded area on the right-hand side plot is the region excluded by LEP constraints, see eq. (16).

for the following values of the input parameters: $M_{Z'} = 1.5$ TeV, $g'_1 = 0.1 \div 0.5$ (in 0.1 steps) and $M_{\nu_h} = 200$ GeV. While the di-lepton mode is a powerful Z' discovery channel, its sensitivity to the presence of heavy neutrinos is however only indirect, through the Z' width, and in fact very weak, as $\Gamma_{Z'}$ varies never more than 20% or so due to the presence of the new states (recall Fig. 3(c)).

In contrast, multi-lepton signatures carry the hallmark of the heavy neutrinos as the latter enter directly the corresponding decay chains and these are explored here by performing a detailed Monte Carlo (MC) analysis at the benchmark point $M'_{Z'} = 1.5$ TeV, $g'_1 = 0.2$ and $M_{\nu_h} = 200$ GeV. The corresponding total cross section for Z' production and decay into heavy neutrinos is 46.7 fb (for CTEQ6L [13] with $Q^2 = M_{Z'}^2$)³.

Through pairs of heavy neutrinos, other than to fully hadronic decays, which are in-

³ When discussing event rates in the following, we will assume an integrated luminosity of $\mathcal{L} = 100 \text{ fb}^{-1}$.

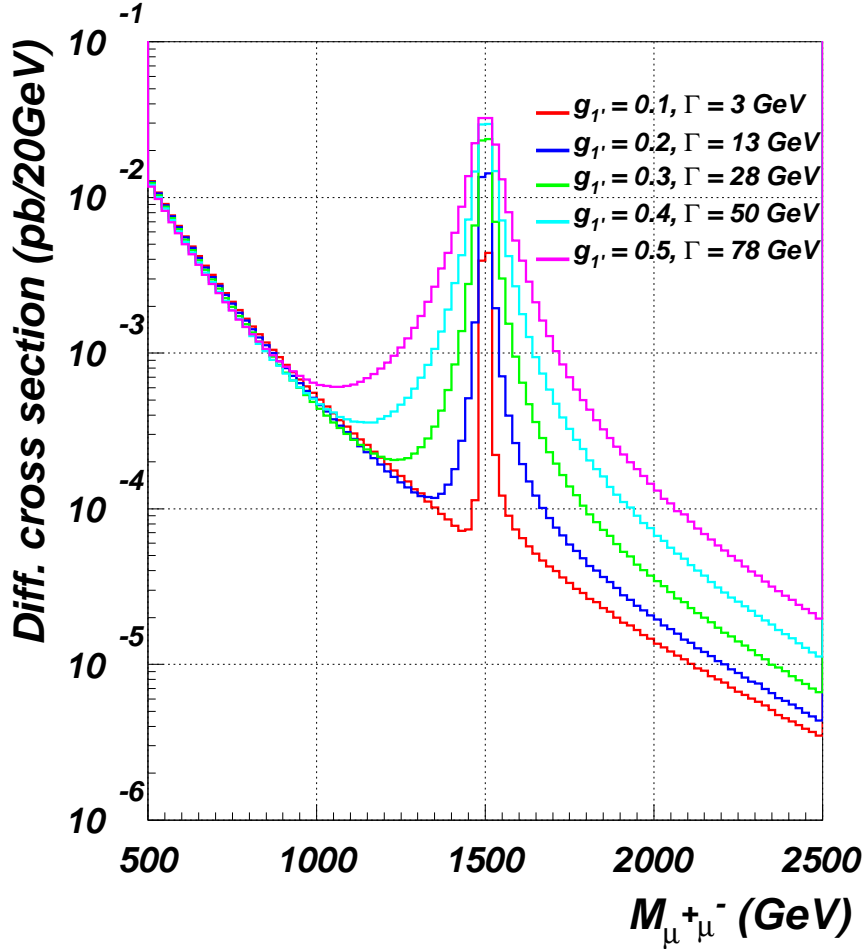


FIG. 7: Differential cross sections for $q\bar{q} \rightarrow Z' \rightarrow \mu^+\mu^-$ at the LHC for $M_{Z'} = 1500$ GeV, $g'_{1'} = 0.1 \div 0.5$ (in 0.1 steps) and $M_{\nu_h} = 200$ GeV as a function of $M_{\mu^+\mu^-}$.

tractable at the LHC (even in presence of the accompanying missing transverse momentum), the Z' can also give rise to 2-, 3- or 4-lepton signatures, for both e and μ in the final state. Amongst the latter, we intend to study here the case of 3-lepton decays. The reason is twofold. On the one hand, we wish to be able to identify heavy neutrino mediation and the presence of only one light neutrino in the 3-lepton mode should enable (transverse) mass reconstruction (contrary to the case of the 4-lepton channel, where two light neutrinos are involved)⁴ On the other hand, we ought to minimise the impact of large backgrounds, so that

⁴ Notice that the 4-lepton final state was discussed in [14]. See instead Ref. [15] for a discussion of the 2-lepton signature.

we neglect here 2-lepton channels (which could easily be overwhelmed by SM DY and $t\bar{t}$ production).

When the heavy neutrino decays via the $l^\mp W^\pm$ mode, with a subsequent leptonic decay of the W^\pm , the charged pair of leptons can carry an invariant mass equal to or lower than the heavy neutrino mass, with the maximum invariant mass configuration occurring when the light neutrino is produced at rest, so that the edge in this distribution corresponds to the ν_h mass. A peak in such a distribution corresponding to the SM-like Z boson, coming from the νZ decay mode for the heavy neutrino will also be present in this distribution. The di-lepton invariant mass distribution is given in Fig. 8. The difference in the two distributions illustrates the effect of taking tau lepton decays that produce muons or electrons into account.

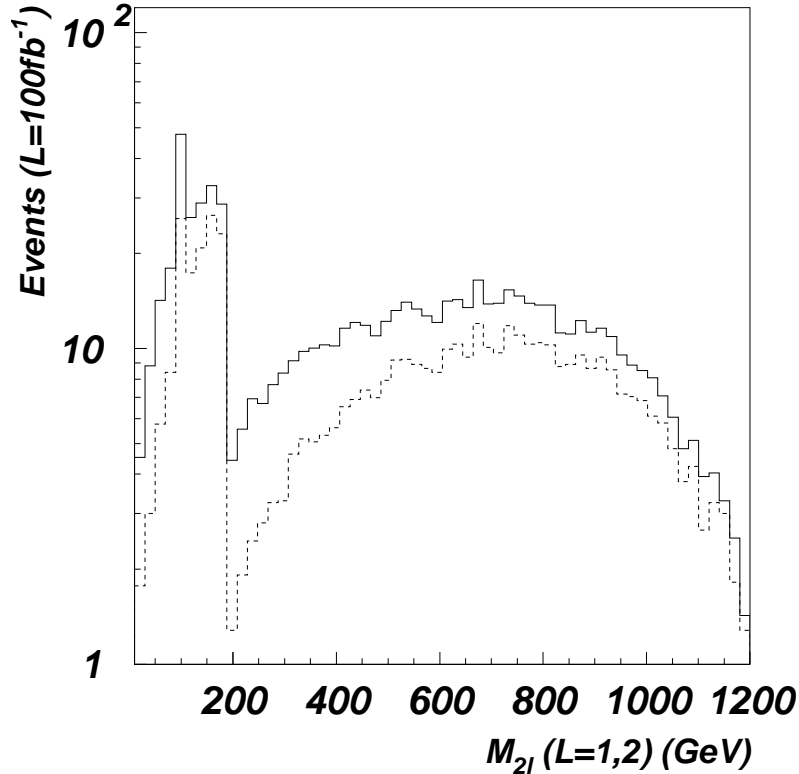


FIG. 8: Invariant mass of the two most energetic leptons in the $Z' \rightarrow 3l$ decay. The dashed line refers to data without taking into account the tau lepton. (Here, $\mathcal{L} = 100 \text{ fb}^{-1}$.)

While the invariant mass distribution can provide some insights into the mass of the intermediate objects, this is not the best observable in the case of the $3l$ -signature, because

the final state neutrino escapes detection. A more suitable distribution to look at is the transverse mass defined in [16], i.e.,

$$m_T^2 = \left(\sqrt{M^2(vis) + P_T^2(vis)} + |\vec{P}_T| \right)^2 - \left(\vec{P}^T(vis) + \vec{P}_T \right)^2, \quad (27)$$

where (vis) means the sum over the visible particles. For the final state considered here we sum over the 3 leptons and 2 jets. The transverse mass distribution is shown in figure 9 where a peak at the Z' mass can be seen. We can also see evidence for the presence of a heavy neutrino by just considering the 2 most energetic leptons and the missing transverse momentum, since this is the topology relevant to a ν_h decay. The results show that this transverse mass peak for the heavy neutrino is likely to be the best way to measure its mass. Both of these configurations are shown in Fig. 9: the signature of this model is that both of the above peaks occur simultaneously. (The different shape for tau-mediated decays is also shown in Fig. 9.)

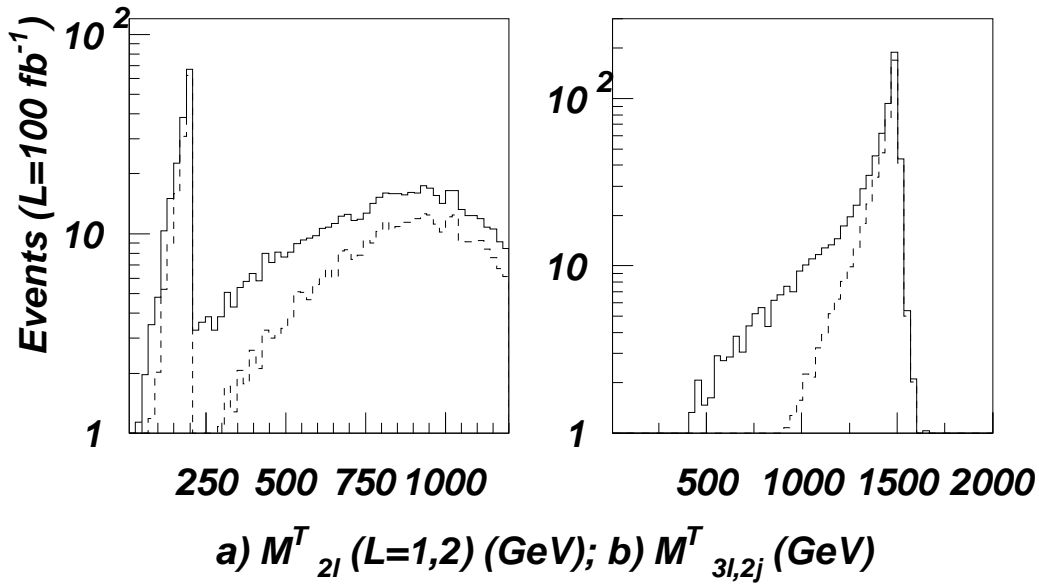


FIG. 9: The transverse mass of the two most energetic leptons (left) and all the visible particles (right) in the $Z' \rightarrow 3l$ decay. The dashed line refers to data without taking into account the tau lepton. (Here, $\mathcal{L} = 100 \text{ fb}^{-1}$.)

The SM background to the 3-lepton signature was studied using CalcHEP. (For simplicity, from now on, we limit ourselves to the case without leptonically decaying τ 's.) Making the

assumption that the Z' peak has already been identified and its mass measured elsewhere (as is likely from $Z' \rightarrow 2l$ decays)⁵, we show that the peak in the M_{2l}^T distribution can be seen despite the initially large backgrounds. This enables one to extract a value for M_{ν_n} . In the evaluation of the background we considered three sources (including generation cuts, to improve efficiency):

- $WZjj$ associated production ($\sigma_{3l} = 246.7$ fb, $l = e, \mu$; $\Delta R_{jj} > 0.5$, $P_{j_{1,2}}^T > 40$ GeV, $|\eta_{j_{1,2}}| < 3$),
- $t\bar{t}$ pair production ($\sigma_{2l} = 29.6$ pb, $l = e, \mu$ (b -quark not decayed); QCD scale = $M_t/2$ to emulate the next-to-leading order cross section; no cuts applied),
- $t\bar{t}l\nu$ associated production ($\sigma_{3l} = 8.6$ fb, $l = e, \mu$; QCD scale = $\sqrt{\hat{s}}$, $P_l^T > 20$ GeV).

In the case of $WZjj$ associated production, three leptons come from the subsequent leptonic decays of the two gauge bosons. This is the main source of background. From $t\bar{t}$ pair production two isolated leptons come from the decay of the W^\pm produced from top decay and one additional, third lepton, could come from semileptonic B-meson decay. This lepton though will be not generically isolated, because of the large boost of the b -quark from top-quark decay. We use this fact to suppress $t\bar{t}$ background. Finally, $t\bar{t}l\nu$ will produce three isolated leptons resulting in a significant background despite the small production cross section.

The first set of cuts we use is designed to impose generic detector angular acceptances, lepton and jet transverse momentum minimal thresholds and to provide isolation for leptons and jets:

⁵ Though notice that in Figs. 13–14 the Z' is well above the background, so that its mass could well be fit – independently of process (26) – in the present channel.

Selection #1

$$\begin{aligned}
|\eta_{l,2,3}| &< 2.5, \\
|\eta_{j,1,2}| &< 3; \\
P_{l_1}^T &> 15 \text{ GeV}, \\
P_{l_{2,3}}^T &> 10 \text{ GeV}, \\
P_{j_{1,2}}^T &> 40 \text{ GeV}; \\
\Delta R_{lj} &> 0.5 \quad \forall l = 1 \dots 3, j = 1, 2, \\
\Delta R_{l,l'} &> 0.2 \quad \forall l, l' = 1 \dots 3, \\
\Delta R_{j,j} &> 0.5;
\end{aligned} \tag{28}$$

where

$$\Delta R \equiv \sqrt{\Delta\eta^2 + \Delta\phi^2}.$$

We evaluate the background at two benchmark points for the signal. For the signal the common parameters are:

$$\begin{aligned}
M_{Z'} &= 1500 \text{ GeV}, \\
g'_1 &= 0.2, \\
m_{\nu_i} &= 10^{-2} \text{ eV}
\end{aligned} \tag{29}$$

and two heavy neutrino masses are considered:

$$M_{\nu_h} = 200 \text{ GeV}, \tag{30}$$

$$M_{\nu_h} = 500 \text{ GeV}. \tag{31}$$

These two benchmark points provide two kinematically very different examples. In the first case the heavy neutrinos are much lighter than the Z' producing highly boosted events. In the second, their mass is comparable to $M_{Z'}/2$, hence close to their production threshold, resulting in minimal boost. From a merely kinematic point of view, all other cases will be somewhere between these two.

Special care should be devoted to the treatment of the $t\bar{t}$ background, given its large production rates which, however, as previously mentioned, can be eliminated by enforcing

a suitable lepton-jet separation. The impact of the first set of cuts on the signals and $t\bar{t}$ background is illustrated in Tab. III. The ΔR_{lj} requirement is indeed extremely effective and reduces this background by a factor of $2 \cdot 10^{-3}$. Contrary, the loss of signal due to this cut is reasonably small. Also note that the signal events with the smaller boost have a higher efficiency for passing the angular isolation cuts.

Cut	$M_{\nu_h} = 200 \text{ GeV}$		$M_{\nu_h} = 500 \text{ GeV}$		$t\bar{t}$	
	# of events	Eff. %	# of events	Eff. %	# of events	Eff. %
no cuts	482.32(10)	100	239.30(10)	100	$1.28 \cdot 10^6$	100
η cuts	346.44(7)	71.8	170.79(7)	71.4	$5.1 \cdot 10^5$	43.9
$\Delta R + P_T$ cuts	68.043(15)	14.1	73.668(31)	30.8	99.699(3)	0.014

TABLE III: Efficiencies of the Selection #1 cuts for the two benchmark signals and the $t\bar{t}$ background, for events with three or more leptons and with two or more jets in the final state for $\mathcal{L} = 100 \text{ fb}^{-1}$. In case of $\Delta R_{jj} < 0.5$ partons were merged into one ‘jet’ at the very beginning of the selection.

Figs. 10–11 show the distributions in M_{jj} , $M_{3\ell jj}^T$, $M_{\ell jj}$ and $M_{2\ell}^T$ after Selection #1 cuts, for the signal with the two heavy neutrino masses, 200 and 500 GeV, that we are considering and the and backgrounds.

In signal events both jets come from the W^\pm therefore we apply the following constraint:

Selection #2

$$|M_{jj} - M_W| < 20 \text{ GeV}. \quad (32)$$

After the application of this cut the other distributions considered are shown in Figs. 12–13 for the 200 and 500 GeV heavy neutrino masses, respectively (here, we now also show the difference between the $M_{2\ell}^T$ and $M_{\ell jj}$ distributions). From these plots it is clear that transverse mass $M_{3\ell jj}^T$ provides good discrimination between signal and background. The

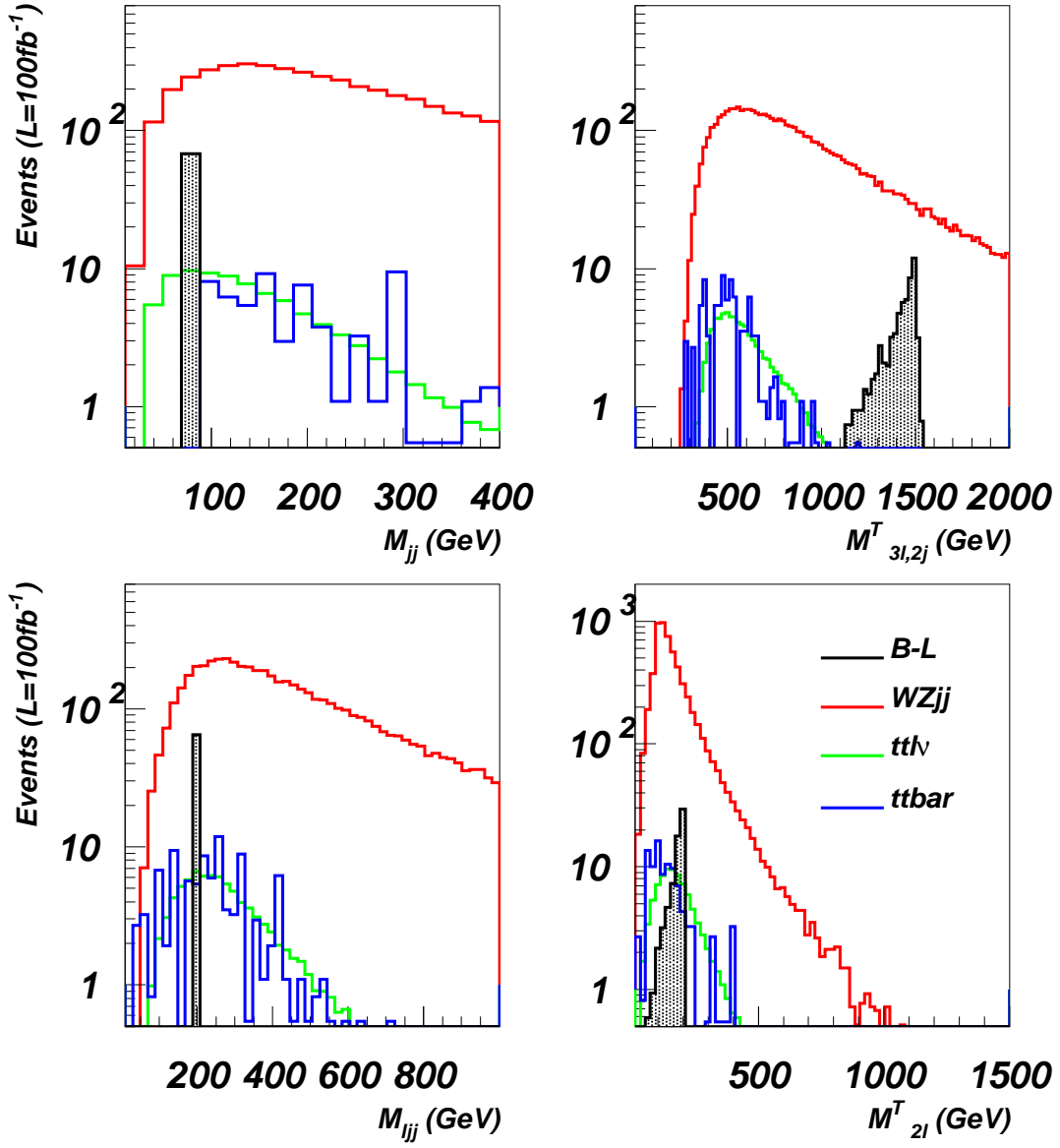


FIG. 10: Signal ($M_{\nu_h} = 200$ GeV) and background distributions after the Selection #1 cuts. (Here, $\mathcal{L} = 100 \text{ fb}^{-1}$.)

following cut is then used to further suppress the background.

Selection #3

$$|M_{3l2j}^T - M_{Z'}| < 250 \text{ GeV}. \quad (33)$$

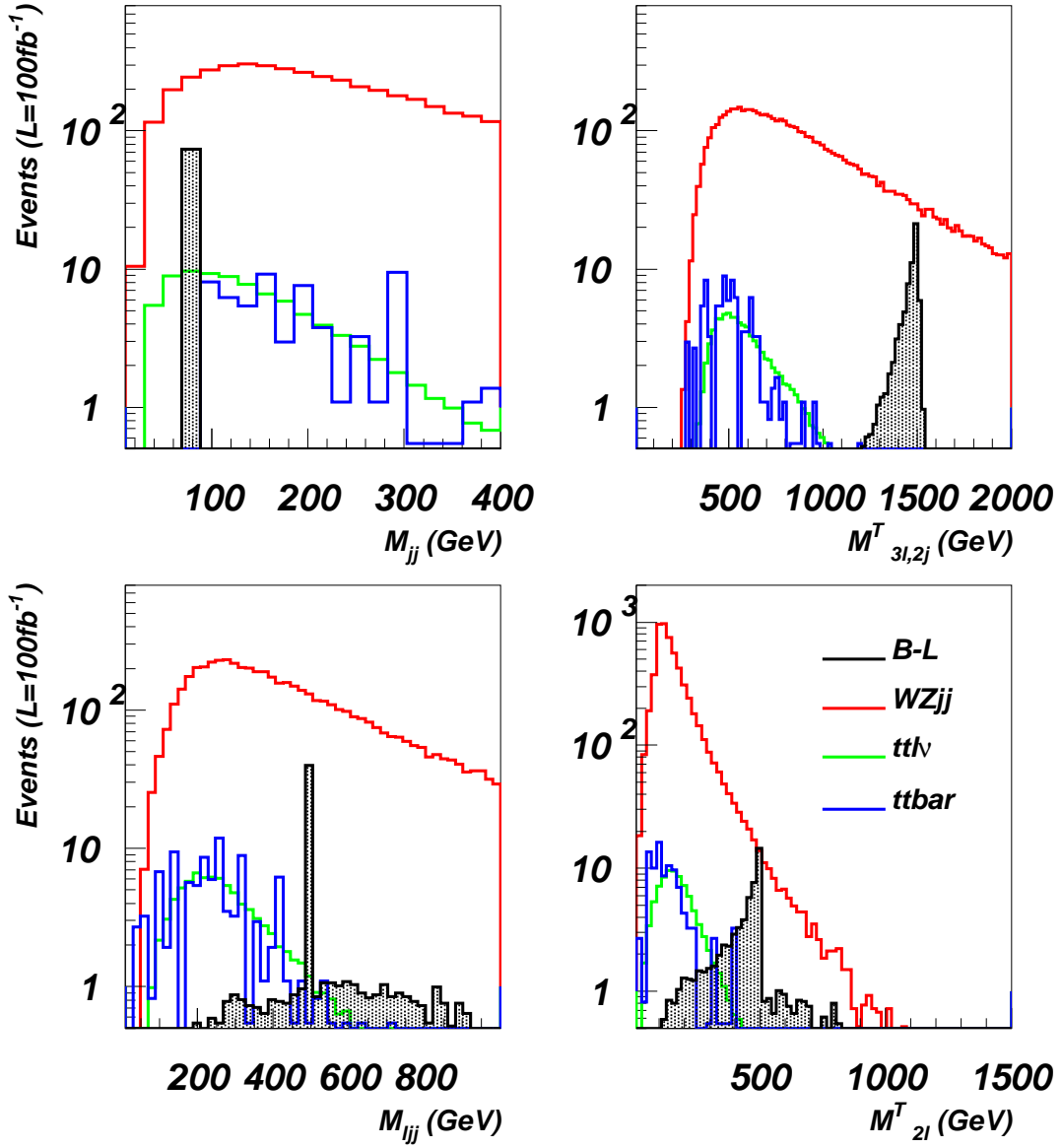


FIG. 11: Signal ($M_{\nu_h} = 500$ GeV) and background distributions after the Selection #1 cuts. (Here, $\mathcal{L} = 100 \text{ fb}^{-1}$.)

After this set of cuts we end up with a very clean signal for both a 200 and 500 GeV ν_h mass in the di-lepton transverse mass distribution, in fact practically free from background, as shown in Fig. 14. Notice that this $M_{2\ell}^T$ variable was formed from the two closest (in ΔR_{ll}) leptons since they are likely to originate from the same boosted ν_h (unlike Fig. 9 – where

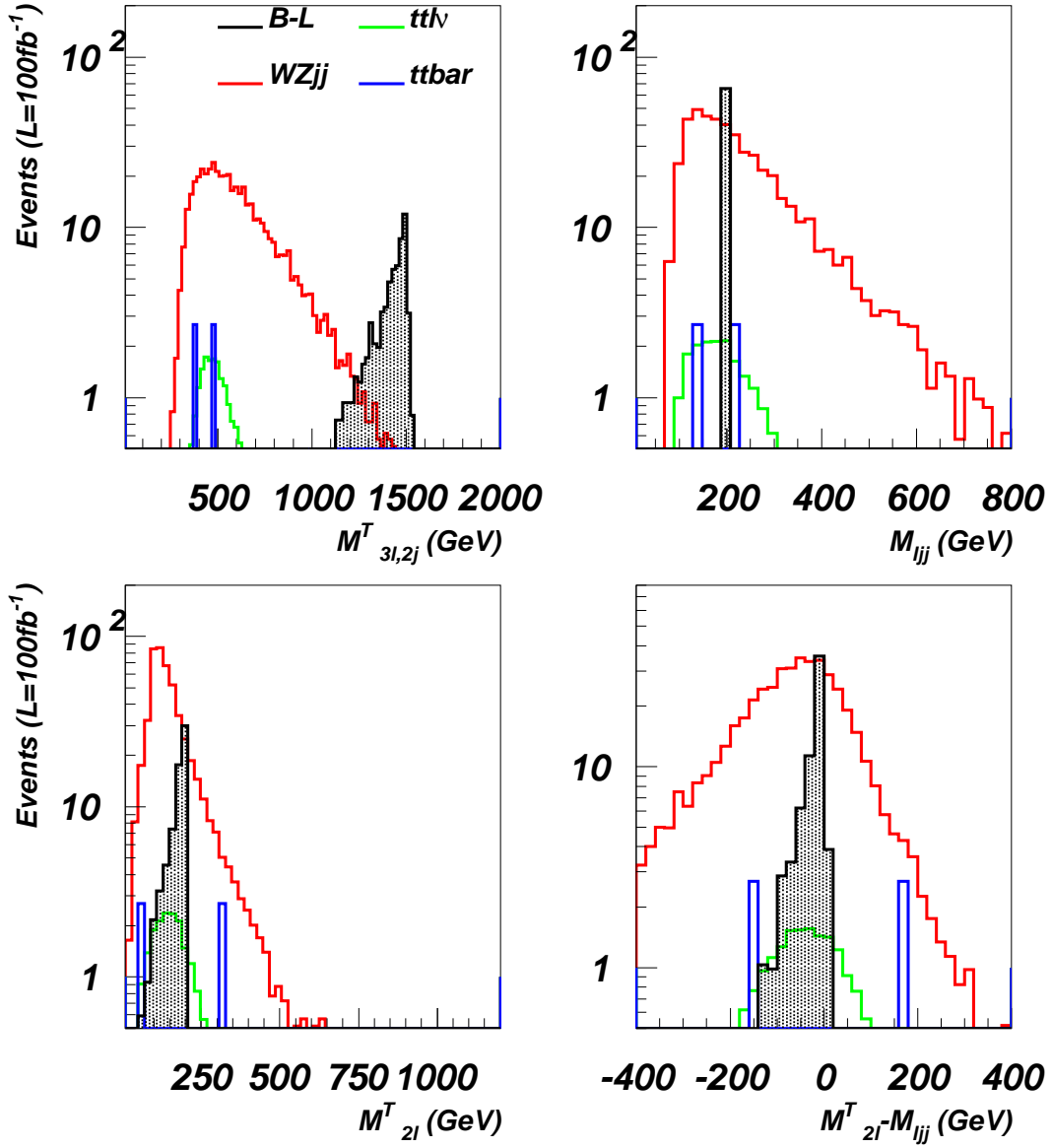


FIG. 12: Signal ($M_{\nu_h} = 200$ GeV) and background distributions after the Selection #1 and #2 cuts. (Here, $\mathcal{L} = 100 \text{ fb}^{-1}$.)

the two most energetic leptons were used.)

In order to establish the signal we finally select events around the visible M_{2l}^T peak, by requiring:

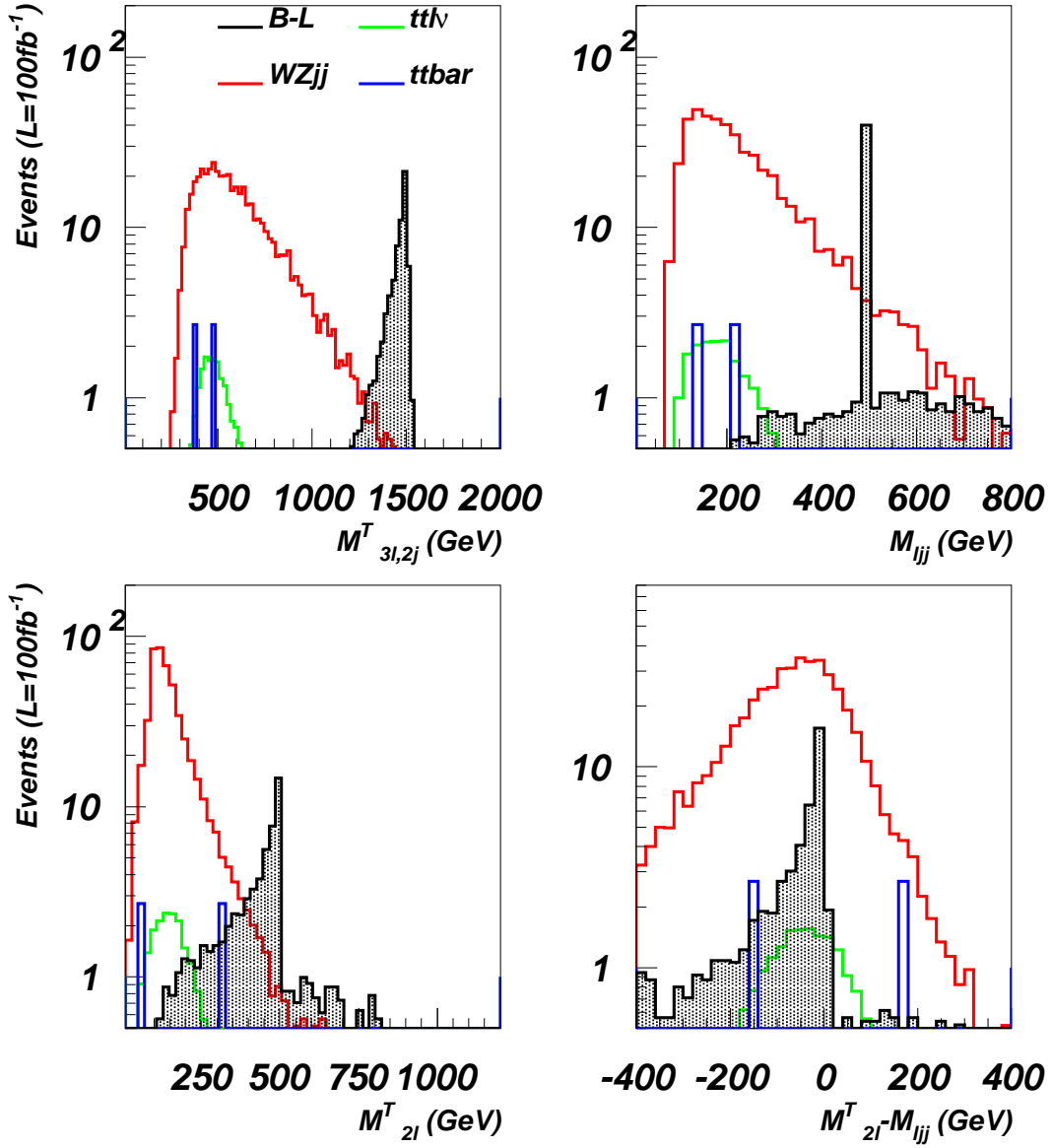


FIG. 13: Signal ($M_{\nu_h} = 500$ GeV) and background distributions after Selection #1 and #2 cuts. (Here, $\mathcal{L} = 100 \text{ fb}^{-1}$.)

Selection #4

$$0 < M_{2l}^T < 250 \text{ GeV} \quad \text{or} \quad 400 \text{ GeV} < M_{2l}^T < 550 \text{ GeV}, \quad (34)$$

depending on the benchmark signal under consideration. The efficiencies of the Selection

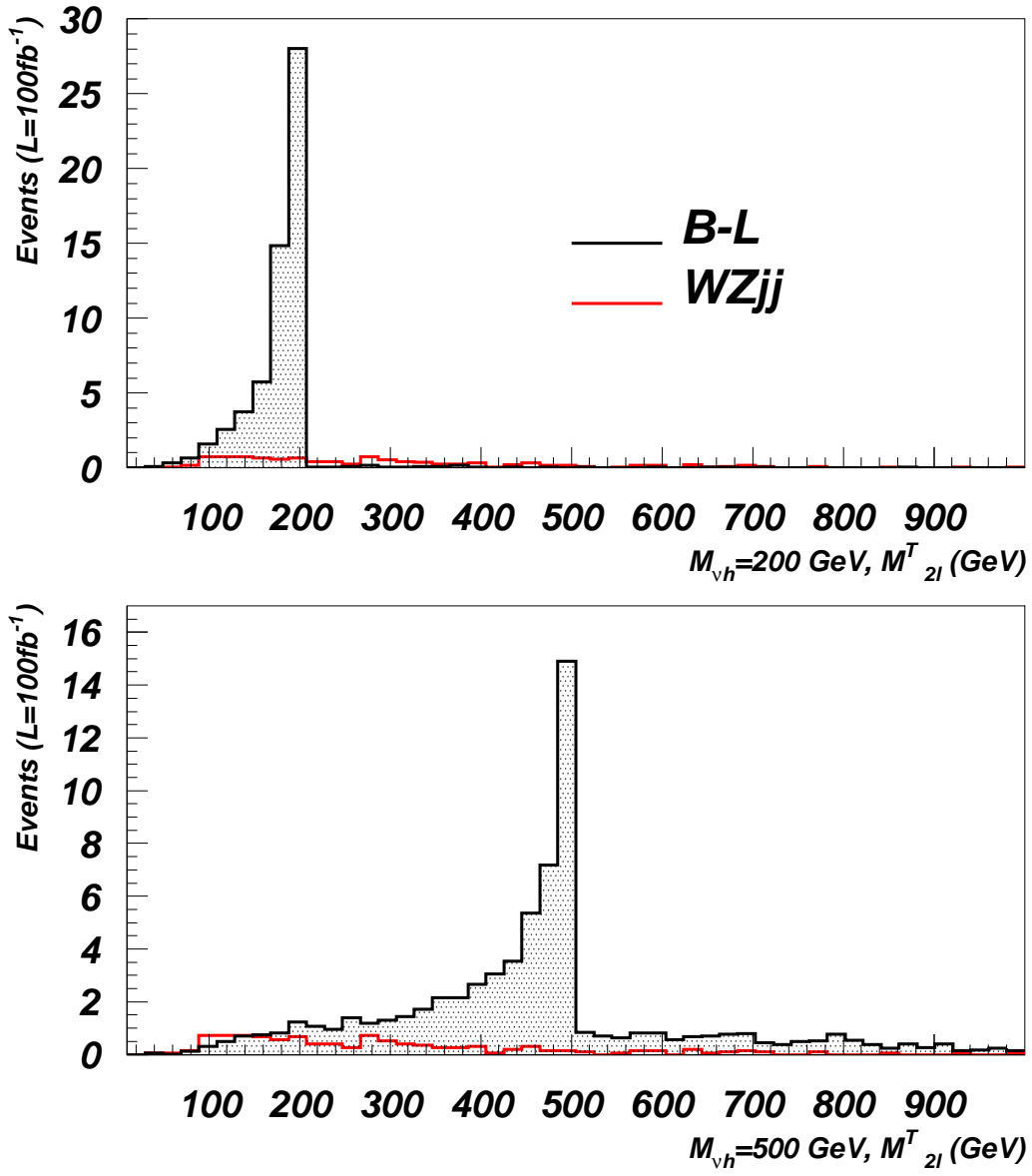


FIG. 14: Signal ($M_{\nu_h} = 200\text{ GeV}$, top, and $M_{\nu_h} = 500\text{ GeV}$, bottom) and background distributions after the Selection #1, #2 and #3 cuts. (Here, $\mathcal{L} = 100\text{ fb}^{-1}$.)

#1–4 cuts, are given in Tab. IV. This summary clearly confirms the feasibility of the extraction of both signals after even less than 100 fb^{-1} of accumulated luminosity.

$$M_{\nu_h} = 200 \text{ GeV}$$

Cuts	Ev. Signal	Eff. %	Ev. $WZjj$	Eff. %	Ev. $t\bar{t}$	Eff. %	Ev. $t\bar{t}l\nu$	Eff. %	S/\sqrt{B}
1	68.043(15)	100	5875.02(24)	100	99.699(3)	100	89.14(16)	100	0.87
2	68.043(15)	100	498.83(2)	8.5	5.3822(2)	5.4	19.38(3)	21.8	2.97
3	58.842(13)	86.5	10.5755(4)	12.7	0	0.8	0.0667(1)	2.2	18.0
4	56.038(12)	94.1	4.4881(2)	67.6	0	56.4	0.03047(5)	64.8	26.3

$$M_{\nu_h} = 500 \text{ GeV}$$

Cuts	Ev. Signal	Eff. %	Ev. $WZjj$	Eff. %	Ev. $t\bar{t}$	Eff. %	Ev. $t\bar{t}l\nu$	Eff. %	S/\sqrt{B}
1	73.668(31)	100	5875.02(24)	100	99.699(3)	100	89.14(16)	100	0.95
2	73.668(31)	100	498.83(2)	8.5	5.3822(2)	5.4	19.38(3)	21.8	3.22
3	68.833(29)	93.4	10.5755(4)	12.7	0	0.8	0.0667(1)	2.2	21.1
4	46.337(20)	66.0	2.87857(1)	7.1	0	8.7	0.00952(2)	10.1	27.6

TABLE IV: Signal ($M_{\nu_h} = 200 \text{ GeV}$ at the top and $M_{\nu_h} = 500 \text{ GeV}$ at the bottom) and background events per $\mathcal{L} = 100 \text{ fb}^{-1}$ and efficiencies following the sequential application of Selection #1–4 cuts.

IV. CONCLUSIONS

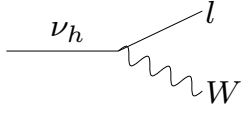
We have analyzed the LHC discovery potential in the Z' and heavy neutrino sector of a (broken) $U(1)_{B-L}$ enlarged SM also encompassing three heavy (Majorana) neutrinos and found that novel signals can be established. The most interesting new signature involves three leptons (electron and/or muons), two jets plus missing transverse momentum coming from a Z' decay chain into heavy neutrinos. Various mass distributions (both invariant and transverse) can be used to not only extract the signal after a few years of LHC running, but also to measure the Z' and heavy neutrino masses involved. This is possible through DY production and decay via $q\bar{q} \rightarrow Z' \rightarrow \nu_h\nu_h$. In fact, for a large portion of the parameter space of our $B-L$ model, the heavy neutrinos are rather long-lived particles, so that they produce displaced vertices in the LHC detectors, that can be distinguished from those induced by b -quarks. In addition, from the simultaneous measurement of both the heavy neutrino mass

and decay length one can estimate the absolute mass of the parent light neutrino, for which at present, only limits exist.

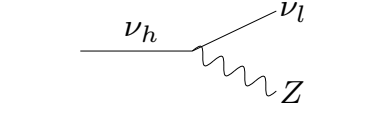
This work has used a MC simulation based on a CalcHEP implementation of the $B - L$ model. The analysis has been done at the parton level though we have verified that our results are stable against the implementation of typical ATLAS/CMS hadronic and electromagnetic calorimeter energy resolution effects. As benchmark scenarios of the $B - L$ model we have chosen two that should be accessible at the LHC, having a Z' mass and fermion couplings not far beyond the ultimate reach of Tevatron and LEP and displaying two extreme relative conditions between the Z' and heavy neutrinos, that is, one with the latter produced at rest and the other highly boosted in the Z' direction.

APPENDIX: FEYNMAN RULES FOR HEAVY NEUTRINO INTERACTIONS

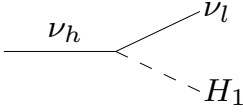
In this Appendix, we list the Feynman rules involving the heavy neutrino of the $B - L$ model considered. The intervening quantities are defined in the main text.



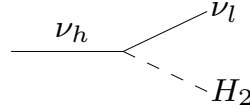
$$\frac{\sqrt{2}e}{4 \sin \vartheta_W} \sin \alpha_\nu$$



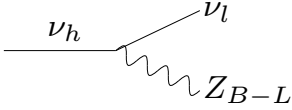
$$-\frac{e}{4 \sin \vartheta_W \cos \vartheta_W} \sin 2\alpha_\nu$$



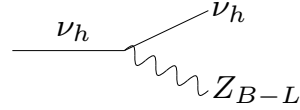
$$\frac{1}{2x} \left(-\sqrt{2}xy^\nu c_\alpha \cos 2\alpha_\nu + M_{\nu_h} \sin 2\alpha_\nu s_\alpha \right)$$



$$\frac{1}{2x} \left(-\sqrt{2}xy^\nu s_\alpha \cos 2\alpha_\nu - M_{\nu_h} \sin 2\alpha_\nu c_\alpha \right)$$



$$g'_1 \sin 2\alpha_\nu$$



$$g'_1 \cos 2\alpha_\nu$$

where $y^\nu = \frac{\sqrt{2}m_{\nu_l}M_{\nu_h}}{v}$, $\sin 2\alpha_\nu = -2\frac{y^\nu \frac{v}{\sqrt{2}}}{\sqrt{4(y^\nu \frac{v}{\sqrt{2}})^2 + M_{\nu_h}^2}}$, $\cos 2\alpha_\nu = \frac{M_{\nu_h}}{\sqrt{4(y^\nu \frac{v}{\sqrt{2}})^2 + M_{\nu_h}^2}}$.

-
- [1] W. Buchmuller, C. Greub and P. Minkowski, *Phys. Lett. B* **267**, 395 (1991).
- [2] P. Minkowski, *Phys. Lett. B* **67** (1977) 421; M. Gell-Mann, P. Ramond and R. Slansky, in *Supergravity*, eds. P. Van Nieuwenhuizen and D. Freedman (North-Holland, Amsterdam, 1979), p. 315; T. Yanagida, in *Proceedings of the Workshop on the Unified Theory and the Baryon Number in the Universe*, eds. O. Sawada and A. Sugamoto (KEK, Tsukuba, 1979), p. 95; S.L. Glashow, in *Quarks and Leptons*, eds. M. Lèvy et al. (Plenum, New York 1980), p. 707; R.N. Mohapatra and G. Senjanović, *Phys. Rev. Lett.* **44** (1980) 912.
- [3] M. Fukugita and T. Yanagida, *Phys. Lett. B* **174** (1986) 45.
- [4] For a review see, e.g.: M. Trodden, *Rev. Mod. Phys.* **71** (1999) 1463.
- [5] S.F. King and T. Yanagida, *Prog. Theor. Phys.* **114** (2006) 1035.
- [6] L. Basso, *A minimal extension of the Standard Model with B–L gauge symmetry*, (Master Thesis, Università degli Studi di Padova, 2007), at http://www.hep.phys.soton.ac.uk/~l.basso/B-L_Master_Thesis.pdf; S. Khalil, *J. Phys. G* **35** (2008) 055001.
- [7] A. Belyaev, L. Basso, S. Moretti, G.M. Pruna and C.H. Shepherd-Themistocleous, in progress.
- [8] A. Pukhov, arXiv:hep-ph/0412191.
- [9] A.V. Semenov, arXiv:hep-ph/9608488.
- [10] P.H. Chankowski, S. Pokorski and J. Wagner, *Eur. Phys. J. C* **47** (2006) 187; F. del Aguila, G.D. Coughlan and M. Quirós, *Nucl. Phys. B* **307** (1988) 633 [Erratum-ibid. *B* **312** (1989) 751].
- [11] M. Carena, A. Daleo, B.A. Dobrescu and T.M.P. Tait, *Phys. Rev. D* **70** (2004) 093009.
- [12] G.L. Fogli, E. Lisi, A. Marrone and A. Palazzo, *Prog. Part. Nucl. Phys.* **57** (2006) 742; G.L. Fogli *et al.*, *Phys. Rev. D* **75** (2007) 053001.
- [13] See: <http://durpdg.dur.ac.uk/hepdata/pdf.html>.
- [14] K. Huitu, S. Khalil, H. Okada and S. K. Rai, *Phys. Rev. Lett.* **101** (2008) 181802.
- [15] W. Emam and S. Khalil, *Eur. Phys. J. C* **522** (2007) 625.
- [16] V. Barger, T. Han and R.J.N. Phillips, *Phys. Rev. D* **36** (1987) 295.